Article

Enhancement and Performance Analysis for Modified 12 Sector-Based Direct Torque Control of AC Motors: Experimental Validation

Mussaab M. Alshbib [1], Ibrahim Mohd Alsofyani [2,*] and Mohamed Mussa Elgbaily [3,4]

1   Mechatronics and Laboratory Engineering Department, Sham University, Aleppo 11566, Syria
2   Department of Electrical and Computer Engineering, Ajou University, World cup-ro 206, Yeongtong-gu, Suwon 16499, Republic of Korea
3   Wolfson Centre for Magnetics, School of Engineering, Cardiff University, Cardiff CF24 3AA, UK
4   Instrumentation & Electrical Division, Gas Transmission and Supply Department, Sirte Oil Company for Production, Manufacturing of Oil and Gas, Marsa Al Brega 385, Libya
*   Correspondence: alsofyani@ajou.ac.kr; Tel.: +82-10-9560-0049

Abstract: Direct torque control (DTC) is a promising control algorithm that is characterized by simplicity and effective performance for the AC motors drive systems. The design of the switching table is an important issue that directly affects the performance of the motor drive. The majority of the prior literature relies on the researcher's knowledge when establishing the voltage vectors of the switching table to be applied to the inverter. Consequently, torque and flux ripples can still be large. In this paper, a modified twelve sector-based DTC is proposed to improve the AC motor drive. The proposed drive system offers several contributions, such as very low torque ripple reduction, faster dynamics, and reduced stator flux ripples compared to the classical DTC. Additionally, the proposed controller can provide high robustness at very low speed under parameter variation. The analytically developed switching table also contributes to reducing the switching frequency ratio between 40% to 50%. The aim of the aforementioned improvements is to obtain a quiet operation of the induction motor without vibration or audible noise. Simulation results of the proposed method were performed in MATLAB/Simulink environment. Furthermore, for the sake of validation and effectiveness of the method, experimental tests were conducted using dSPACE based platform. Finally, a fair comparison of both the proposed and classical methods was performed that revealed the superiority of the proposed strategy.

Keywords: direct torque control; voltage vectors; switching table; twelve sectors

1. Introduction

The DTC algorithm, which was proposed by Takahashi and Noguchi in 1986 [1], appeared as an alternative solution to the Field Oriented Control (FOC) algorithm. DTC is divided according to its presence in the literature into two main parts: First, Direct Self Control (DSC) as known is based on switching tables [2] which is characterized by a variable switching frequency. Secondly, DTC is based on a solution called Deadbeat that has a fixed switching frequency and requires a Pulse Width Modulation (PWM) stage [3]. The classic DTC is based on the direct selection of the voltage vector from a switching table in order to fulfill control requirements [4]. In spite of the simplicity and cost effective performance of such algorithm, it still suffers from many disadvantages, the most important of which are high torque, flux, and current ripples, as well as variable switching frequency. Research has focused primarily on minimizing these disadvantages as much as possible. Lookup table with sector modifications, developed-torque or flux controller, and combined DTC-VC are the most recently approved aspects in order to improve the algorithm's performance. In terms of sectors modification, many researchers have increased the number of sectors to

be twelve sectors, eighteenth sectors, twenty-four sectors. Researchers [5,6] used a twelve sectors DTC algorithm with a two-level flux regulator and a four-level torque regulator. Thus, low oscillation amplitude could be obtained. Digital Signal Processor (DSP) In the Loop implementation of an enhanced DTC was performed in [7] with 12 sectors and three-levels hysteresis controllers. Fast dynamics-flux and torque could be achieved, as well as less values of current distortion compared to classical DTC. However, difficulties in the calculations of the speed block were present. Twelve sectors-based DTC with fuzzy logic speed controller was implemented in [8]. In spite of the Total Harmonic Distortion (THD) improvement for both the flux and the torque, the system was tested only at low speeds range not at medium or high speeds. A modified switching table of DTC algorithm was proposed in [9] in order to obtain lower hysteresis boundary conditions using active vectors with zero ones. Twelve sectors and two switching tables were used, one for low speeds while the other for high speeds. In [10], enhancement performance of the DTC of an interior Permant Magnet Synchronous Motor (PMSM) over the wide speed range in terms of higher capability of the motor torque was achieved. Twelve sectors and three hysteresis controllers were used with such method in order to control the flux, toque, and voltage. The torque regulator had four levels, while the rest of the regulators only have two levels. In [11], a T-type inverter is proposed with twelve sectors to reduce the torque and flux ripples with retaining the fast dynamics. Torque ripples was less 20% than ripples in conventional DTC. However, increased losses could be observed due to the presence of Silicone Carbide (SiC) MOSFETS. 18 sectors based DTC with an improved stator flux observer was proposed in [12] and two levels of both the flux and torque comparators. Torque ripples could be reduced at low speeds, while the authors didn't check the performance at high speeds. In addition, the stator flux response was not plotted at either low or high speed. Reference [13] suggested an 18 sector based-DTC with twelve virtual space vectors for an induction motor. The system's performance was evaluated in both directions of speed. However, the torque and stator flux responses disappeared from the simulation and experimental results. High dynamic torque response and least sector-stator flux droop with constant frequency torque regulator was supposed in [14] for the induction motor. A modified stage to obtain the stator flux error was suggested in the research [15] to increase the torque dynamics. The modified flux error depends on the torque error, the sector, and the two components of the flux vector. This method was characterised by simplicity. However, the steady state characteristics were not fully investigated. In [16], two dynamic hysteresis torque bands (DHTB-I, II) were proposed to improve the DTC algorithm of the induction motors. The objective of the two methods for developing the flux or torque controller is to achieve flux control at low speeds and near zero speeds. Fast Torque Control of DTC was proposed for the induction motor in [14], leading to constant switching frequency. This approach is enhanced by increasing the bandwidth of the torque-loop [17]. A fuzzy regulator was proposed in [18,19] to guarantee the suitable voltage vector. Although of reduction in both torque and flux ripples in [18], the practical implementation was lost, as well as the increase of the manual tuning gains (which are six). Reduction of both the torque and flux ripples was achieved using a fuzzy based switching table with twelve sectors [20]. A comprehensive analysis of the genetic and practical swarm optimization (PSO) algorithms for DTC was proposed in [21] to reduce torque ripples and also to increase the robustness and effectiveness of the DTC approach. In [22], twelve sector-based DTCs for Permant Magnet Synchronous Generator (PMSG) were performed. The stator flux and torque were controlled by hysteresis controllers with two and three levels of hysteresis, respectively. However, speed response analysis was not conducted across different speed ranges.

Different from the existing methods in the same area, a modified twelve-sector DTC is proposed to obtain optimal performance of the DTC drive. The developed control scheme makes several contributions, including the reduction of torque ripple, faster torque dynamics, and reduced stator flux ripple up to 75%. Furthermore, the proposed DTC is capable of providing higher robustness at a very low speed under resistance variation and contributes to reducing the switching frequency by 50%. Additionally, an extensive analysis

of the proposed control algorithm under various operating conditions, such as load and speed, is provided. The effectiveness of the proposed DTC is verified by simulation and experimental results and compared with the conventional DTC.

The sections of this article are structured as follows; Section 2 presents an overview of the basics of the DTC algorithm. Then, an analytical investigation of the proposed twelve sectors of the DTC is performed in Section 3. Simulation results and experimental validation are provided in Sections 4 and 5, respectively. The performance evaluation with traditional DTC is carried out in Section 6. Finally, the conclusion is drawn in Section 7.

2. Principle of DTC Algorithm

Figure 1 illustrates the block diagram of the classical DTC algorithm. The stator flux amplitude Φ_s and the electromagnetic torque T_{em} are controlled by using two independent hysteresis controllers. Each of Φ_s and T_{em} are estimated based on the stator currents, the inverter pulses, and the dc-link voltage E [23]. The estimated stator flux and torque are compared with the reference values in order to obtain the errors which are entered into the hysteresis regulators. The output of the flux comparator, the torque comparator, and the sector index determines the voltage vector should be selected from a switching table to drive the inverter supplying the motor [24].
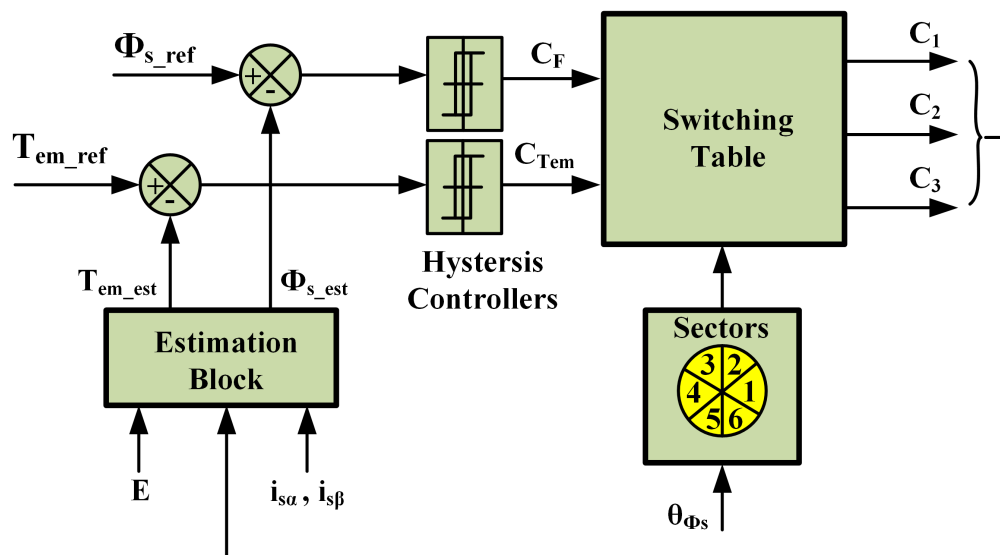

Figure 1. The block diagram of the classical DTC.

The switching table used in the traditional DTC algorithm is shown in Table 1 [6]:

Table 1. The switching table for the classical DTC.

Torque	Flux	Sectors					
Error	Error	S_1	S_2	S_3	S_4	S_5	S_6
0	0	V_5	V_6	V_1	V_2	V_3	V_4
	1	V_6	V_1	V_2	V_3	V_4	V_5
1	0	V_3	V_4	V_5	V_6	V_1	V_2
	1	V_2	V_3	V_4	V_5	V_6	V_1

In the stationary reference frame, denoted by the superscript (s), the derivative of the stator flux vector is given in (1):

$$\frac{d\Phi_s^s}{dt} = \underline{V}_s^s - R_s \underline{i}_s^s \tag{1}$$

where, R_s is the phase stator resistance, $\underline{is}_s^s$ is the stator current vector, and $\underline{V}_s^s$ is the stator voltage vector. The two components of the stator voltage vectors are calculated via the DC-link and the inverter switching pulses of the inverter transistors C_a, C_b, C_c as in (2) and (3) [25]:

$$v_{s\alpha} = \sqrt{\frac{2}{3}} E \left[C_a - \frac{1}{2}(C_b + C_c) \right] \tag{2}$$

$$v_{s\beta} = \sqrt{\frac{1}{2}} E [C_b - C_c] \tag{3}$$

The position of the stator flux vector is given in (4):

$$\theta_{\Phi s} = \arctan\left(\frac{\Phi_{s\beta}}{\Phi_{s\alpha}}\right) \tag{4}$$

The amplitude of the torque is obtained via the stator and the rotor fluxes amplitudes and the angle (γ) between them as shown in (5) [26].

$$T_{em} = \frac{p L_m}{\sigma L_s L_r} \Phi_s \Phi_r \sin\gamma \tag{5}$$

where p is the number of pole pairs; L_m, L_r, and L_s are the mutual, rotor, and stator self inductances, respectively; σ is the leakage factor.

3. The Analytical Investigation of the Proposed Twelve Sectors DTC

The classical strategy represented in Table 1 exploited four effective vectors out of the six inverter voltage vectors. However, vector V_i and the opposite vector V_{i+3} have unignored effect on both the stator flux and the torque. The effect of these two vectors can be entered into an improved switching table that differs from the traditional table with modification of the stator flux sectors. The six classical sectors will be divided into twelve sectors so that each new sector occupies 30° of the coordinate plane ($\alpha^s - \beta^s$) as shown in the Figure 2, the main purpose of the analytical study is to correctly devise the switching table used in the improved strategy, i.e., the determination and the accurate effect of the voltage vectors on both the change of error for both the torque and the stator flux. It is worth mentioning that the torque regulator is selected with four levels while the stator flux regulator was maintained at two levels.
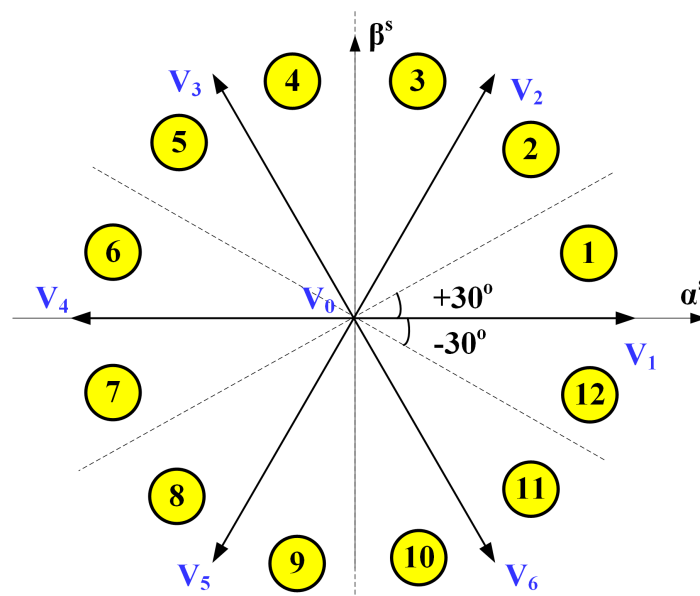

Figure 2. Dividing the stator flux path into twelve sectors.

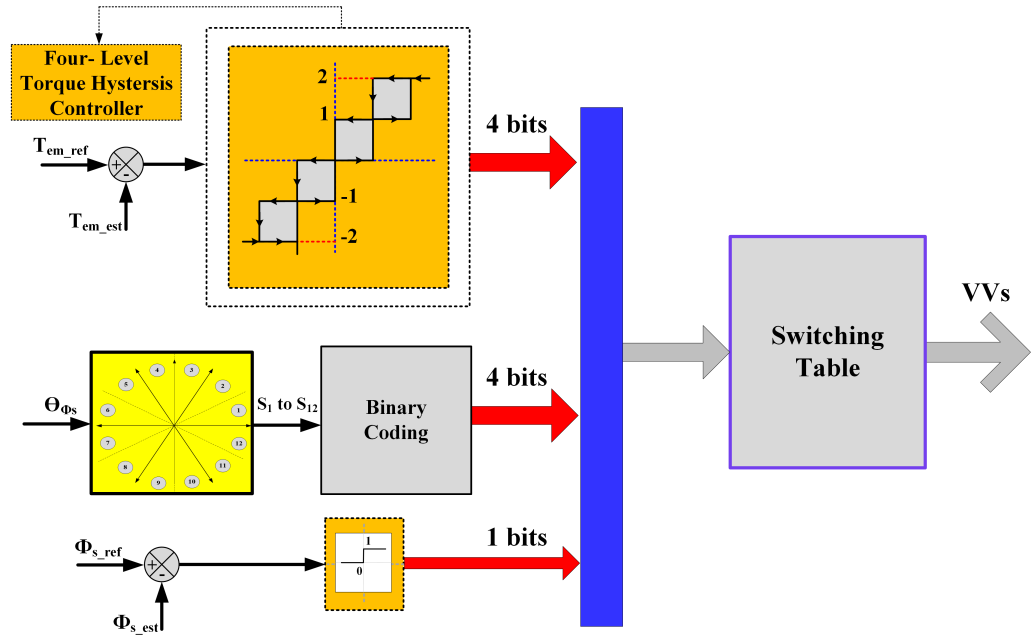Figure 3 shows the block diagram of the proposed twelve sectors based DTC method.

Figure 3. The block diagram of the proposed DTC.

In order to perform the analytical study, the stator flux vector will be oriented towards to the α-coordinate axis. The two components of the voltage vector in the synchronous reference frame (α, β) are given in (6) and (7).

$$V_{s\alpha} = \sqrt{\frac{2}{3}}\, \text{Ecos}\left(\frac{n-1}{3}\pi - \theta_{\Phi s}\right) \tag{6}$$

$$V_{s\beta} = \sqrt{\frac{2}{3}}\, \text{E}\sin\left(\frac{n-1}{3}\pi - \theta_{\dot{\Phi}s}\right) \tag{7}$$

where, n is the sector index.

The errors of the stator flux and the torque are in (8) and (9).

$$E_{\Phi s} = \Phi_{S\_ref} - \Phi_S \tag{8}$$

$$E_{T_{em}} = T_{em\_ref} - T_{em} \tag{9}$$

The derivatives of the two previous errors can be written as in (10) and (11) [27].

$$C_{\Phi_s} = -\frac{d\Phi_{s\_est}}{dt} = -\frac{\text{Re}[\underline{V}_s\Phi_s^*] - R_s\,\text{Re}[\underline{i}^*{}_s\underline{\Phi}_s]}{\Phi_s} \tag{10}$$

$$C_{T_{em}} = -\frac{dT_{em\_ref}}{dt} = \left(\frac{1}{\sigma\tau_s} + \frac{1}{\sigma\tau_r}\right)T_{em} - \frac{pLm}{L_sL_r}\,\text{Im}\left[\underline{V}_s\Phi^*_{r\_est} - j\omega\underline{\Phi}_s\Phi^*_{r\_est}\right] \tag{11}$$

The relation between the rotor flux and the stator flux as in (12).

$$\Phi_r = \frac{Lm}{L_s}\frac{1}{1+j\sigma\tau_r}\Phi_s \tag{12}$$

The two component equations of the stator flux vector in the synchronous reference frame are in (13) and (14) [28].

$$i_{s\alpha} = \frac{1}{L_s} \cdot \frac{1 + \sigma(\tau_r \omega_r)^2}{1 + (\sigma \tau_r \omega_r)^2} \Phi_s \tag{13}$$

$$i_{s\beta} = \frac{1}{L_s} \cdot \frac{1 + \tau_r \omega_r (1 - \sigma)^2}{1 + (\sigma \tau_r \omega_r)^2} \Phi_s \tag{14}$$

The following equations must be fulfilled with all selected vectors in the proposed switching table:

$$E_{\Phi s} \cdot C_{\Phi s} < 0 \quad , \quad E_{Tem} \cdot C_{Tem} < 0 \tag{15}$$

Taking into account the equations (10) and (11), the voltage vectors effects for the twelfth and first sectors were plotted in Figure 4 for three different speeds: Low speed equals 10% ω_n, medium speed 50 % ω_n, and high speed 90% ω_n, respectively.

- **At low speed** 10% ω_n: In the twelve sector, all vectors maintain the sign of torque and stator flux over the entire sector except for the vector V_2 which results in a decrease in stator flux for a quarter of the sector, while increasing it in the rest of the sector. As for the vector V_1, it changes the torque sign in a very small part of the sector. However, this effect can be neglected. In the first sector, all vectors maintain the sign of torque and flux over the whole range of the sector, except for V_4, which increases the torque at the end of the sector by a negligible amount as well.
- **At medium speed** 50% ω_n: the situation for the twelfth sector is not different from the previous case, except that the two vectors V_1, V_3 that produce a decrease in torque at the end of the sector, which is greater for the V_3 than for V_1. For the first sector, the effect of the vectors is ideal for torque. However, the vector V_6 decreases the stator flux at the end of the sector by an amount that can be neglected.
- **At high speed** 90% ω_n: For the 12 sectors, the vector V_2 is the only choice for reducing torque. However, this vector decreases the flux at the beginning of the sector while increasing it for the most part of the sector. For the first sector: the two vectors V_2, V_3 have an almost equal effect on the torque in terms of increasing at the beginning of the sector and decreasing in the remaining part of the sector. In order to investigate the effects of the voltage vectors according to the load changes at nominal speed, the analytical results shown in Figure 5 were performed. Three changes of load were tested which are: low load equals 10% of nominal load, medium load equals 50% of the nominal load. For the twelfth sector, it is observed that changing the load did not change the positions of the vectors except for the vector V_3. The effect of this vector rises gradually with the increase of the load, i.e., the degree of decreasing the torque increases with the increase of the load. However, the flux does not changes its sign with this vector. Similarly, for the first sector, as all vectors maintain the same effects with increasing load, except for the vector V_3. At low and medium loads, this vector works to reduce the torque on the entire sector. However, for a nominal load, this vector works to decrease the torque at the first half of the sector while increase it with the remaining half of the sector.

To find out the effect of the stator resistance R_s variation on the position of the vectors, Figure 6 was drawn. Three values of the resistance were selected which are: nominal Rs, 1.5* Rs, 2* Rs. For the twelfth sector, it is observed that the two vectors V_1, V_2 change their effects on the torque in limited values. Their effect in reducing the torque increases more and more with the increase of the resistance. However, for the first sector, the situation is completely optimal, since the vectors did not change their position with the change of the resistance value.
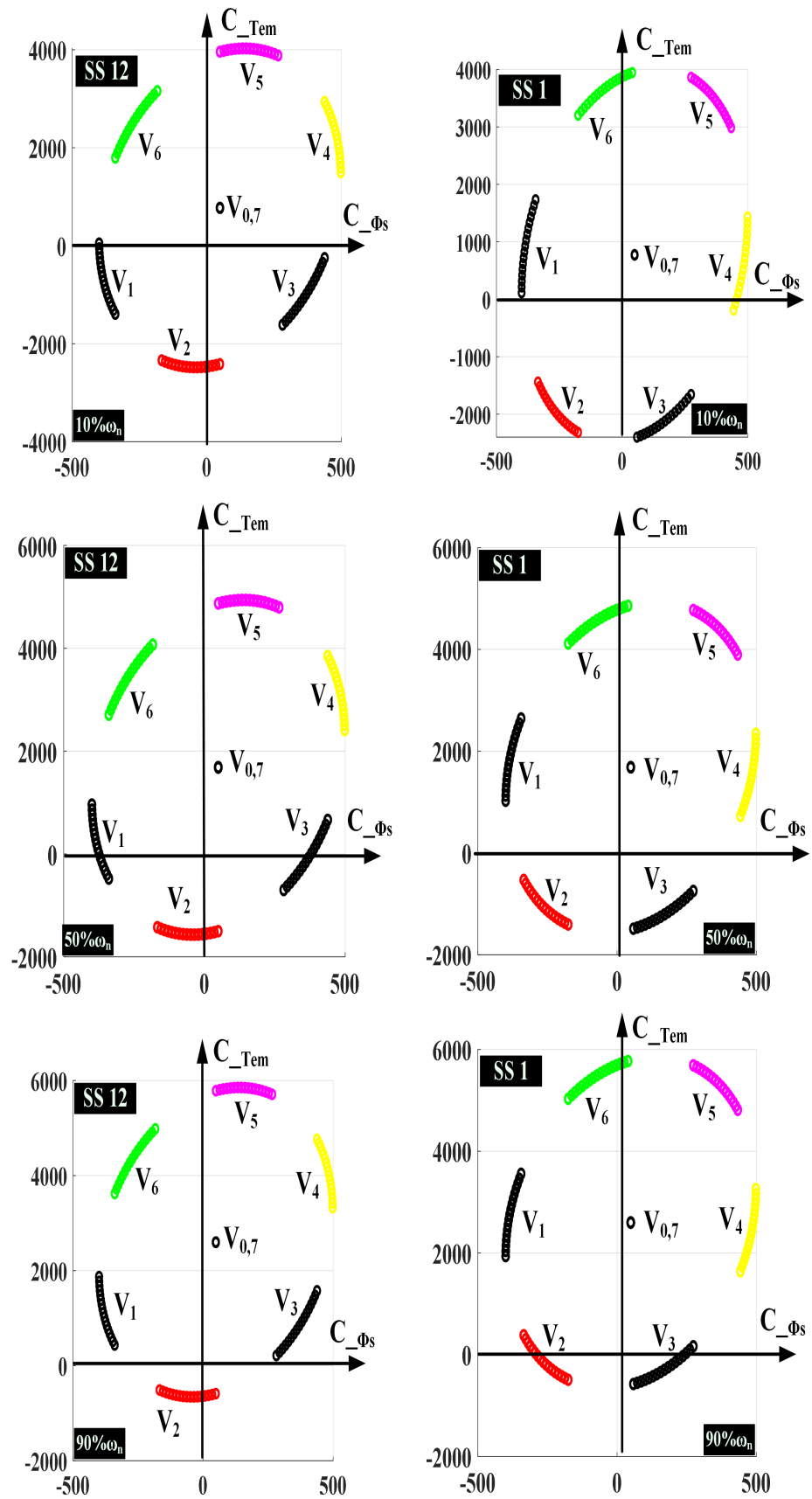
Figure 4. Effect of the voltage vectors on the error variation of both torque and stator flux.
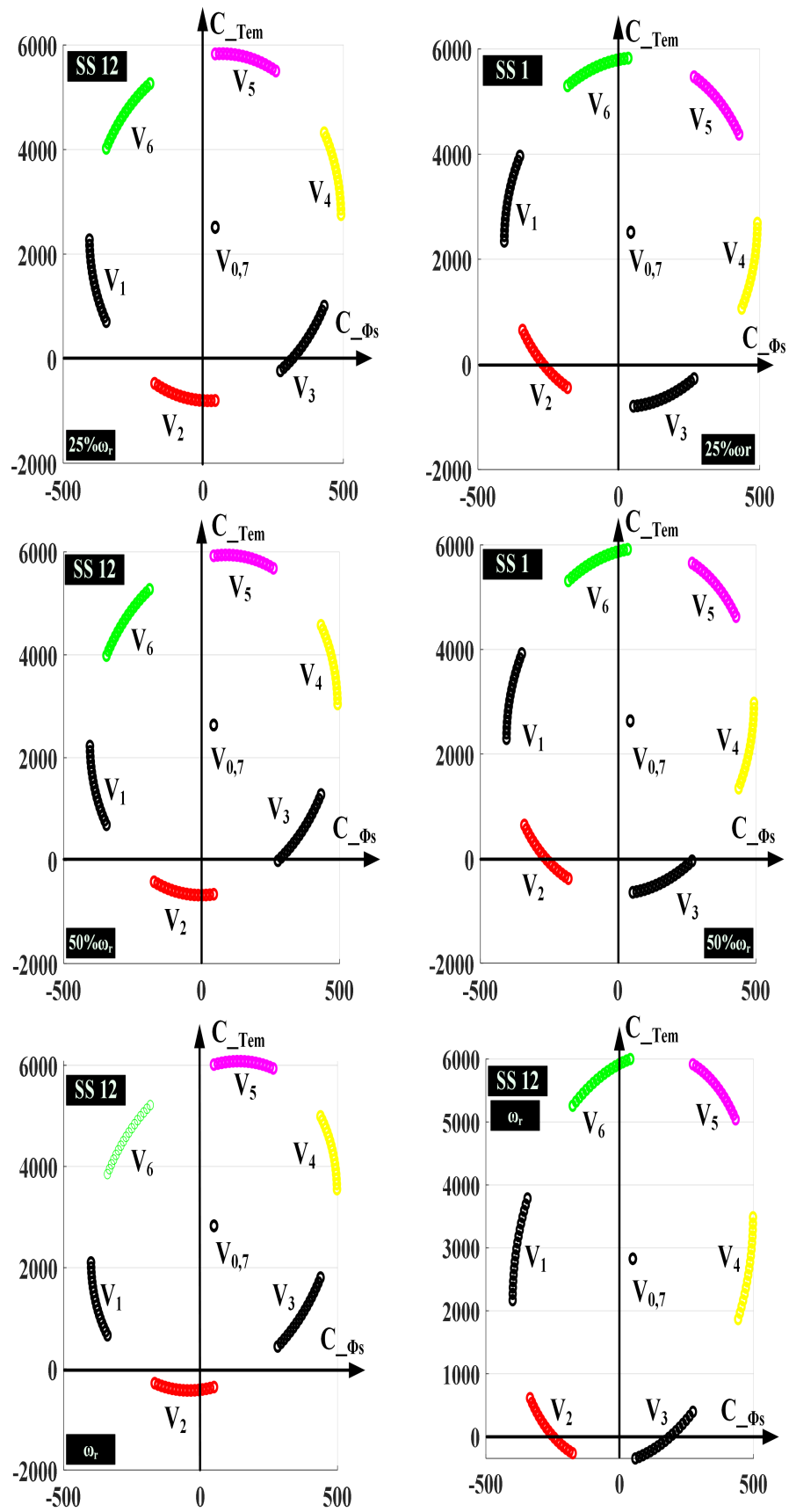
Figure 5. Effect of the voltage vectors on the error variation of both torque and stator flux for different loads.
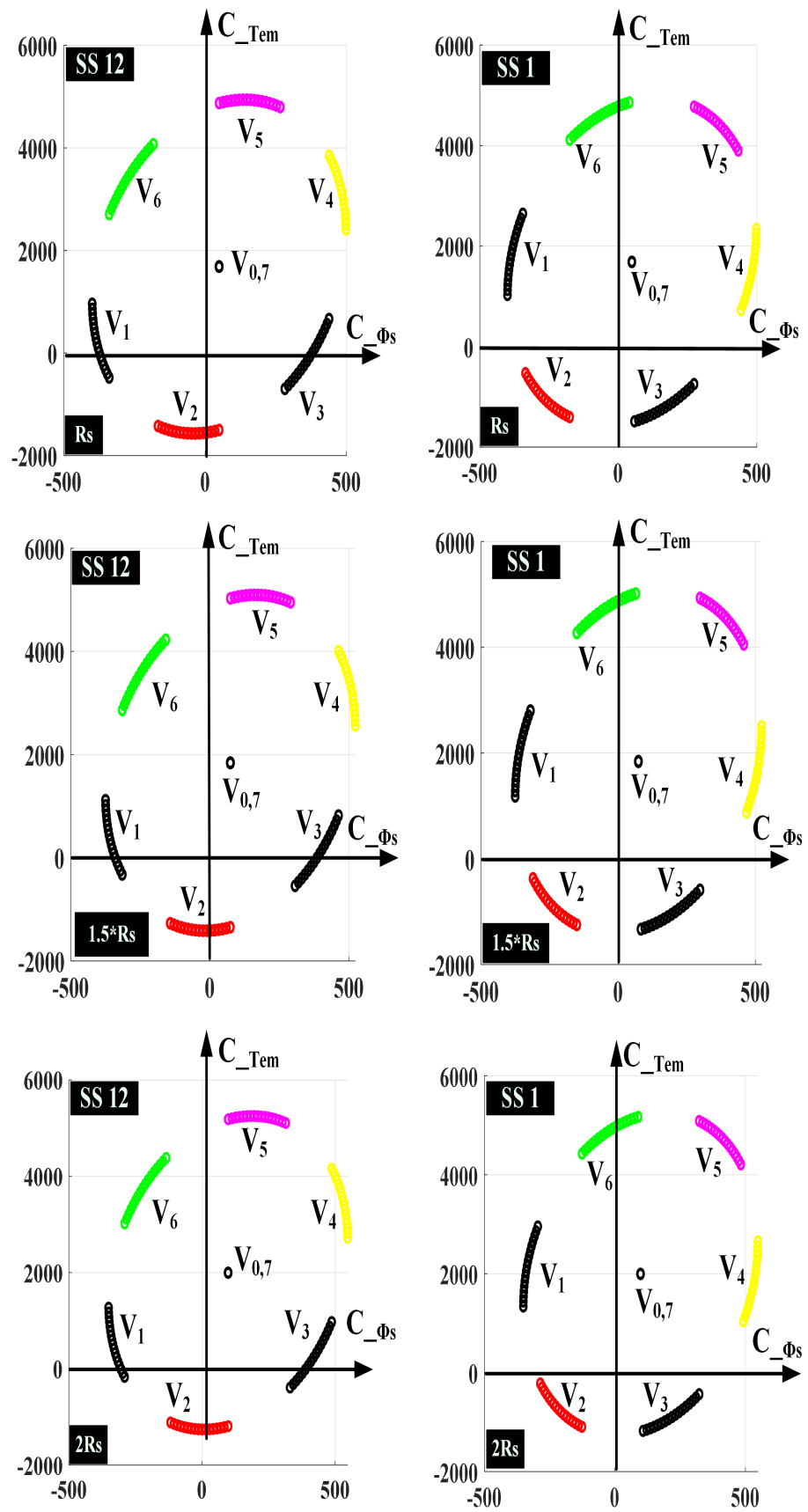
Figure 6. Effect of the voltage vectors on the error variation of both torque and stator flux for Rs variation.

Figure 7 illustrates the effect of the zero voltage vector on the error variation for both the flux and the electromagnetic torque. This effect is analyzed over the whole speed range with no load and full load. The application of the zero voltage vector causes an increase of the error change of the stator flux. In addition, This vector effect is not dependent on the speed range. However, it is dependent on the load range. The effect of this vector is small equals 42.1 Wb/s for the no-load operation. However, it reaches 49.2 Wb/s for the nominal load. So, it is concluded that the application of the zero vector causes a slight decrease in the amplitude of the stator flux, regardless of the speed range. With regard to the change in the torque error, it can be observed that the application of the zero vector causes a positive change in the value of the C_{Tem}. This change increases with the increase of the speed, and is greater with the full load compared to no load. This change ranges within 500–2800 N · m/s for the increasing speed and nominal loads. However, this change decreases to be within the range 0–800 N·m/sec when working with no load. It is concluded that the application of the zero vector causes a decrease in the value of the torque so the amount of torque decrease is greater at high speeds when compared with low speeds.
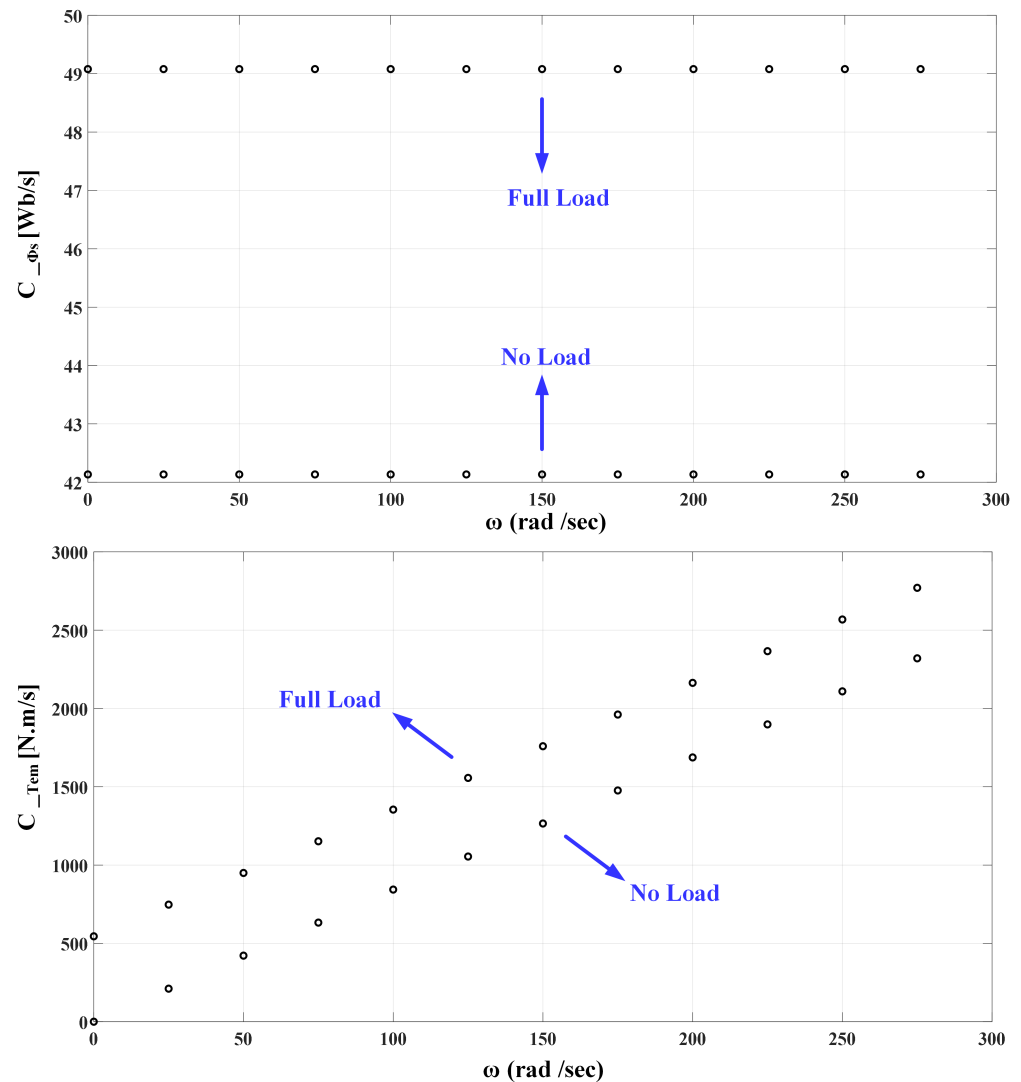

Figure 7. The effect of the zero voltage vector on both the error changes of the stator flux and the torque.

Based on the results of the above-mentioned analytical study, the switching table was derived, as shown in Table 2, for the proposed strategy with 12 sectors, two flux levels and four torque levels. Note that this switching table is not the only option.

Table 2. The switching table of the proposed DTC.

Flux	FD				FI			
Torque	−1	−2	1	2	−1	−2	1	2
SS12	V_5	V_0	V_2	V_2	V_6	V_6	V_1	V_2
SS1	V_5	V_0	V_3	V_3	V_6	V_1	V_2	V_2
SS2	V_6	V_0	V_3	V_3	V_1	V_1	V_2	V_3
SS3	V_6	V_0	V_4	V_4	V_1	V_2	V_3	V_3
SS4	V_1	V_0	V_4	V_4	V_2	V_2	V_3	V_4
SS5	V_1	V_0	V_5	V_5	V_2	V_3	V_4	V_4
SS6	V_2	V_0	V_5	V_5	V_3	V_3	V_4	V_5
SS7	V_2	V_0	V_6	V_6	V_3	V_4	V_5	V_5
SS8	V_3	V_0	V_6	V_6	V_4	V_4	V_5	V_6
SS9	V_3	V_0	V_1	V_1	V_4	V_5	V_6	V_6
SS10	V_4	V_0	V_1	V_1	V_5	V_5	V_6	V_1
SS11	V_4	V_0	V_2	V_2	V_5	V_6	V_1	V_1

However, the designer can adjust the selection of vectors according to the control requirements [29]. The switching table was initially filled in for the twelve and the first sectors. For the rest of the sectors, the task is performed by adding the number one to the vector index applied in the current sector, according to the following sequence:

- The twelfth, second, fourth, sixth, eighth, tenth.
- The first, third, fifth, seventh, ninth, eleventh.

4. Simulation Results

The proposed strategy was simulated in MATLAB/Simulink environment. Runge Kutta solver with fixed step size T_s = 50 µs was set for the simulation calculations. Figure 8 shows the torque response of the proposed strategy for the two directions of the tested motor (its parameters are shown in Appendix A). The torque is well controlled around the nominal reference value ±1.76 N·m. Figure 9 shows both the stator and the rotor fluxes modulus. It can be noted that the stator flux is well regulated around its nominal reference value 1.14 Wb for different steps of the reference torque. The rotor flux is approximately maintained at a constant value. The response of the rotor flux suffers from ripples less than the value of the stator flux because the rotor flux is filtered from the stator flux since the relationship between them is a first-order filter Equation (12) [30]. Figure 10 depicts the three-phase motor currents for various reference torque increments.
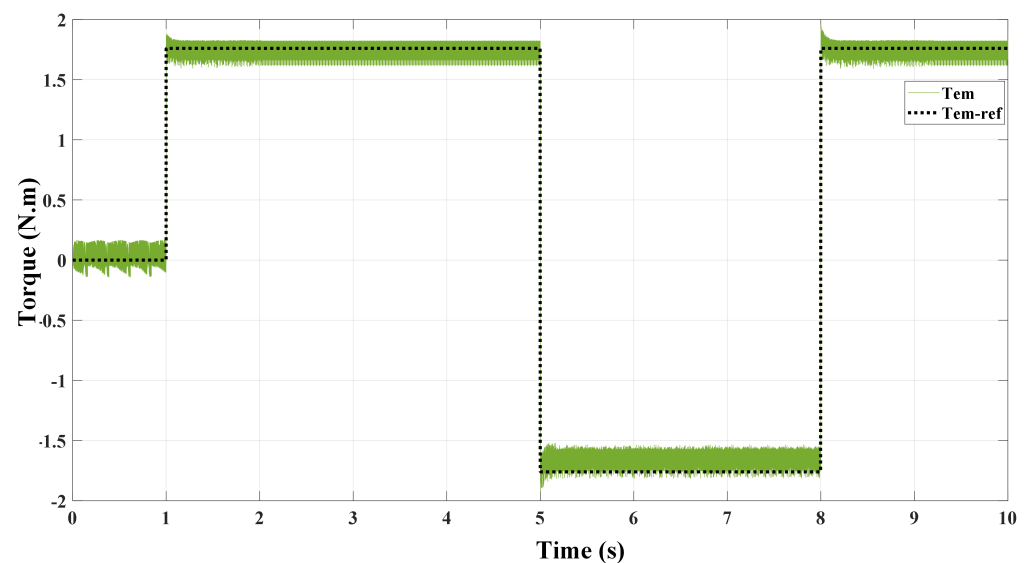

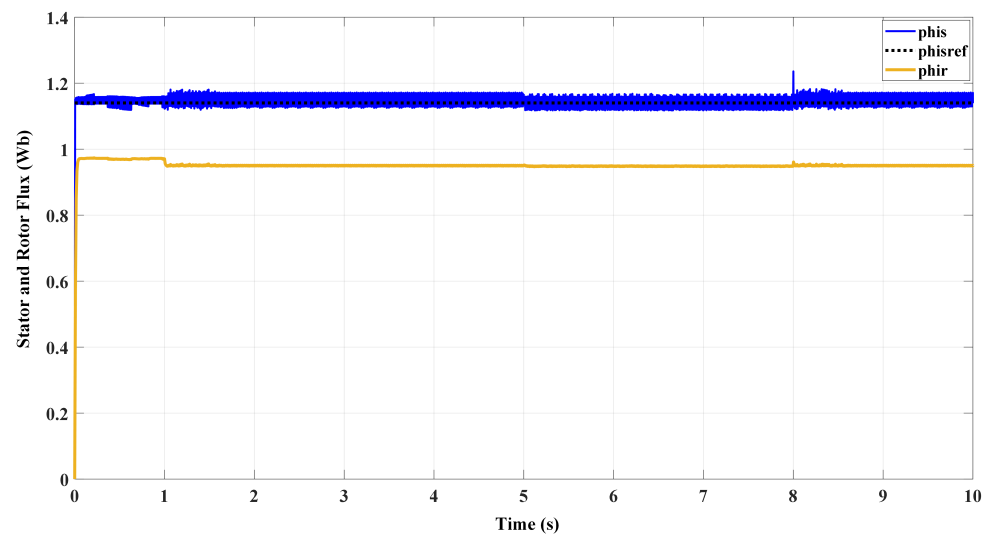**Figure 8.** The torque response in the proposed strategy.

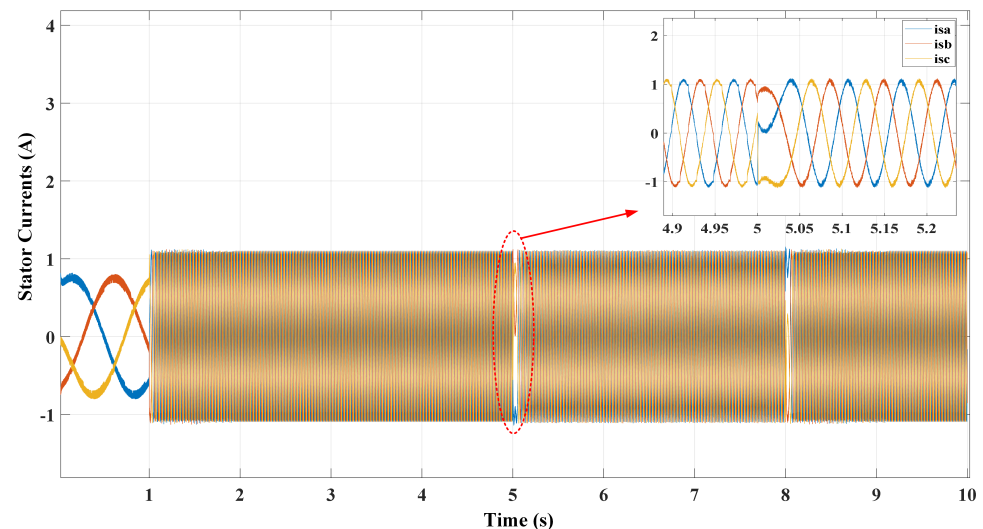**Figure 9.** Responses of the stator and rotor fluxes in the proposed strategy.

Figure 10. Responses of the three-phase stator currents in the proposed strategy.

Due to the precise selection of voltage vectors, it is observed that these currents have low ripples, according to the analytical study conducted for this research. The currents increased from 0.99 A to 1.1 A when the reference torque jump increased from half the nominal to the nominal value. Figure 11 depicts the twelve sectors of the stator flux pattern, with the electrical angle of the rotor indicated as varying from 0 to 2*pi. This figure verifies the proper sequence of the generated sectors as the motor rotor completes its full rotation. Figure 12 compares the transient and steady-state torque responses of the improved twelve sector technique and the conventional strategy. In order to apply successive reference torque jumps, a value of 0.88 N·m equals half the nominal torque, was used as the starting point. A reference torque equal to the nominal torque of 1.76 N·m was applied at 5 s. After 8 s, a reference torque equal to half of the nominal torque was reapplied. It is observed that the transient response of the torque in the enhanced method is faster than in the conventional technique. The improved strategy has a transient response time of 0.4 ms, while the conventional strategy has a response time of 0.5 ms. In contrast, the steady-state response of the torque in the enhanced technique is demonstrably superior to that of the conventional strategy. The amplitude of ripples in the improved strategy is 0.15 N·m, while it is 0.6 N·m in the conventional strategy at roughly 75%.
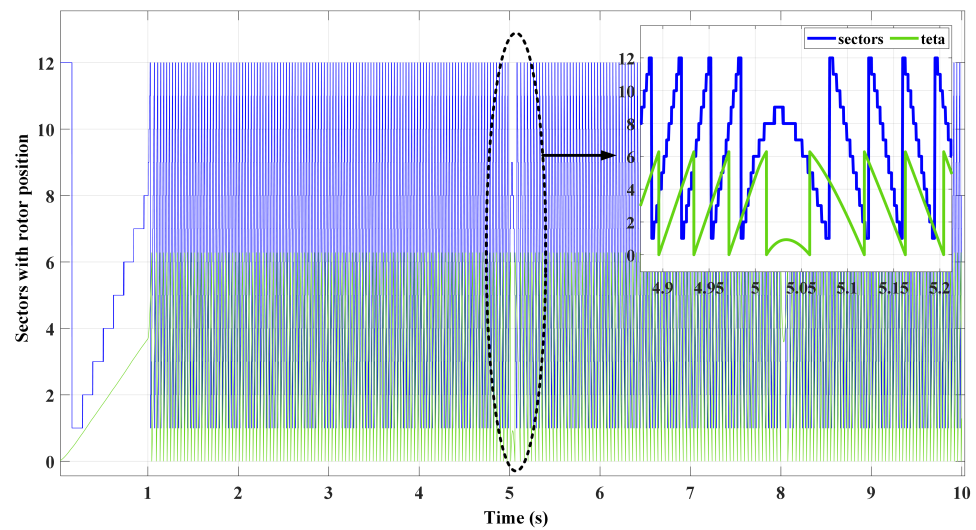
Figure 11. The twelve sectors with the electrical angle of the rotor of the proposed method.
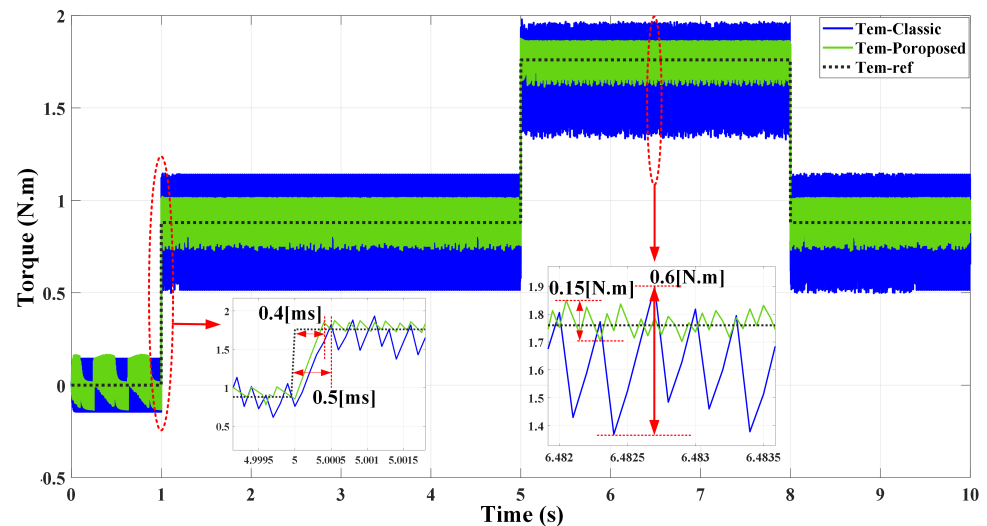

Figure 12. The torque responses in both the classical and improved strategies.

The aforementioned reference torque jumps occurred at 35 rad/s for half the nominal torque, while the speed for the reference nominal torque was 70 rad/s, as seen in Figure 13. Figure 14 shows the comparison of the stator flux response in the improved twelve sectors strategy with the classical strategy in the transient and steady states. It is observed that the transient response of the stator flux in the improved strategy is faster than its counterpart in the classical strategy. The transient response time in the improved strategy is 4 ms, while in the classical strategy is 7 ms. On the other hand, the steady-state response of the stator flux in the improved strategy is clearly better than the classical strategy. For half nominal reference torque, the flux oscillation in the improved strategy was 0.03 Wb while it was 0.06 Wb in the classical strategy. For the nominal reference torque, the flux oscillation in the improved strategy was 0.04 Wb versus 0.06 Wb in the classical strategy. The ratio of reduction of magnetic flux ripples in the improved strategy to the ripples in the classical strategy is 33% to 50% depending on the applied reference torque.
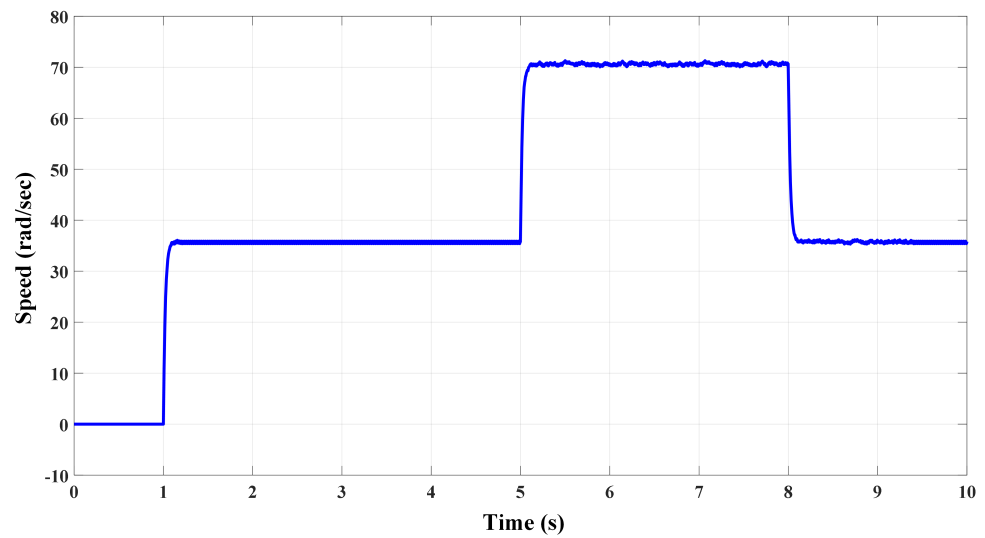
Figure 13. Speed response for different reference jumps of the torque.
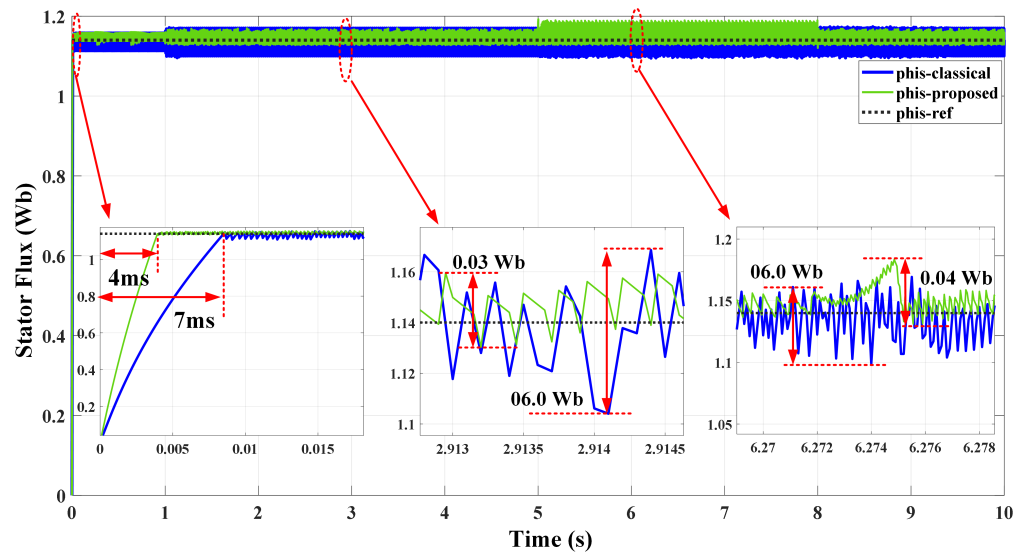

Figure 14. Stator flux response in both the classical and improved strategy.

Figure 15 shows the trajectory of the stator flux vector in both the classical and the improved strategy. It can be seen the obvious improvement resulting from the improved strategy over the entire path of the stator flux vector compared with the classical strategy.
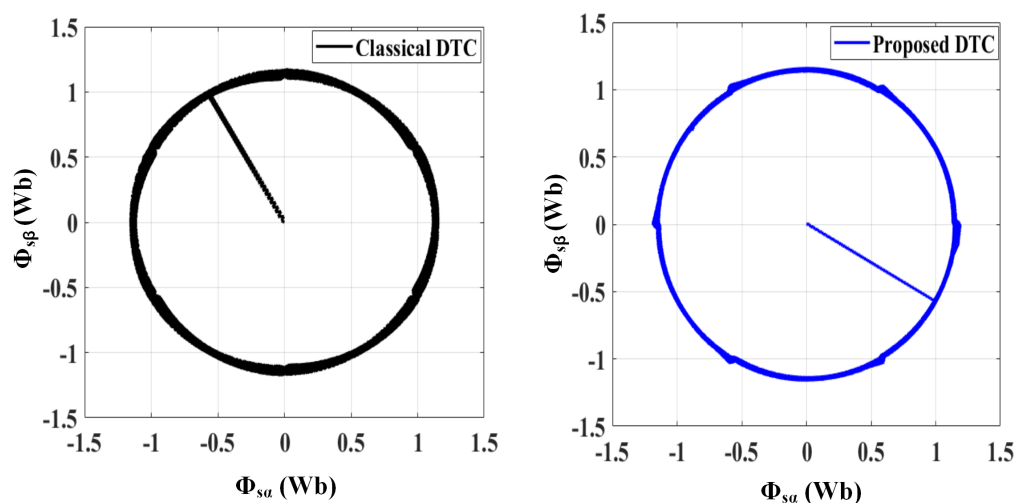
Figure 15. Trajectory of the stator flux vector in both the classical and improved strategy.

In order to test the robustness of the improved strategy toward the variation of the stator resistance, Figure 16 was performed for very low speed equals 5 rad/s. At 3 s, the stator resistance R_s was increased by 100% of its value in both improved and classical strategy. It is noted that the speed response in the improved strategy was not affected by this variation, since the value of the speed oscillation was 0.1 rad/s before and after the variation. However, the classical strategy was significantly affected by the variation of the resistance. Speed oscillation doubled between 0.12 rad/s and 0.24 rad/s before and after the variation, respectively. This confirms that the proposed strategy is more robust than the classical strategy towards the stator resistance variation, especially at low speeds.
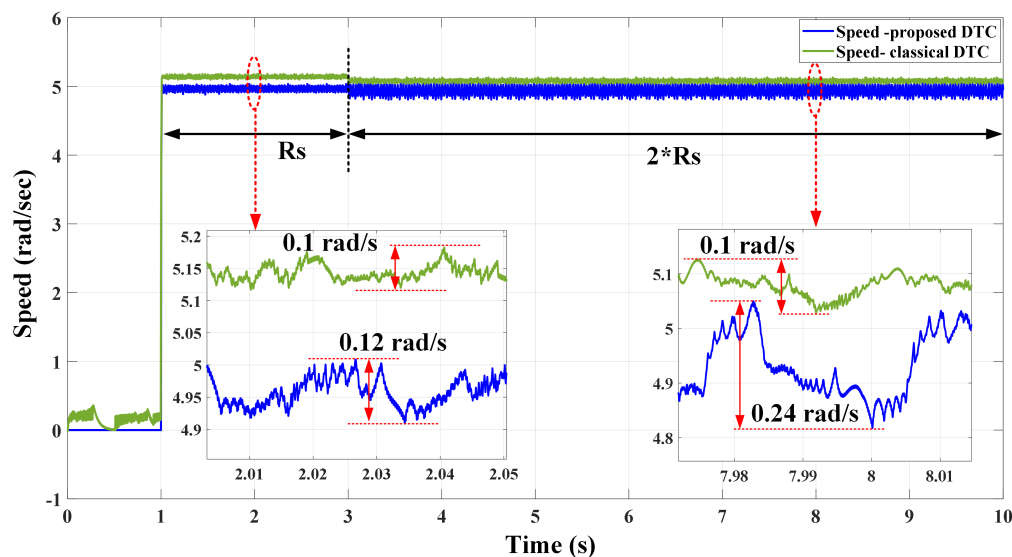

Figure 16. Speed response for Rs variation in both the classical and improved strategy.

Figures 17 and 18 show three-phase motor currents for a very low speed of 5 rad/s in each of the two strategies. It is clear that the ripples within the currents of the improved strategy are significantly less than the ripples within the currents of the classical strategy. This confirms that the performance of the proposed strategy is better than the classical strategy in the range of low speeds close to zero speed.
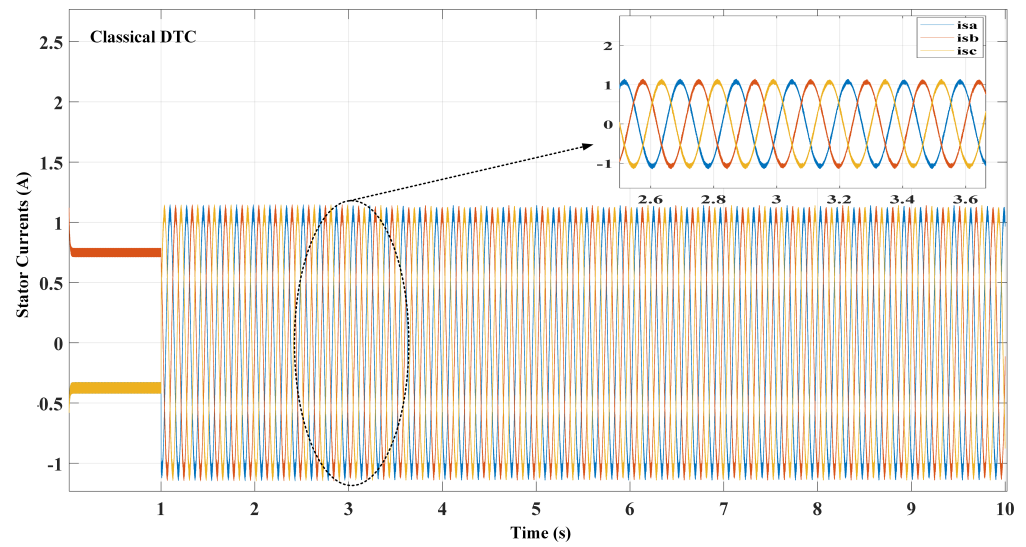
Figure 17. Stator currents of classical DTC for very low speed 5 rad/s.
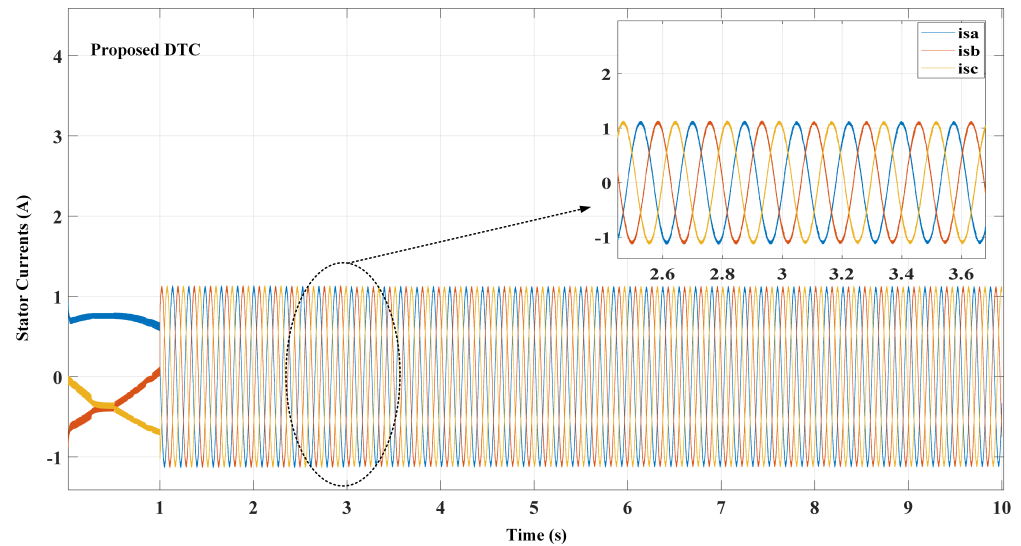

Figure 18. Stator currents of the proposed method for very low speed 5 rad/s.

Figure 19 shows the variation of the switching frequency of the inverter switches over a wide speed range in both the classical and the improved strategy. It is clear that the improved strategy produced lower switching frequency over the entire range of speeds compared to the classical strategy. The largest value of switching frequency at low speed equaled 7.25 kHz in the classical strategy, while it was 3.1 kHz for the improved strategy. For half the nominal speed, the switching frequency in the classical strategy was 5.2 kHz, while its value in the improved strategy was 4.5 kHz. For nominal speed, the switching frequency value in the classical strategy was equal to 2.1 kHz while it was 1.2 kHz in the improved strategy.
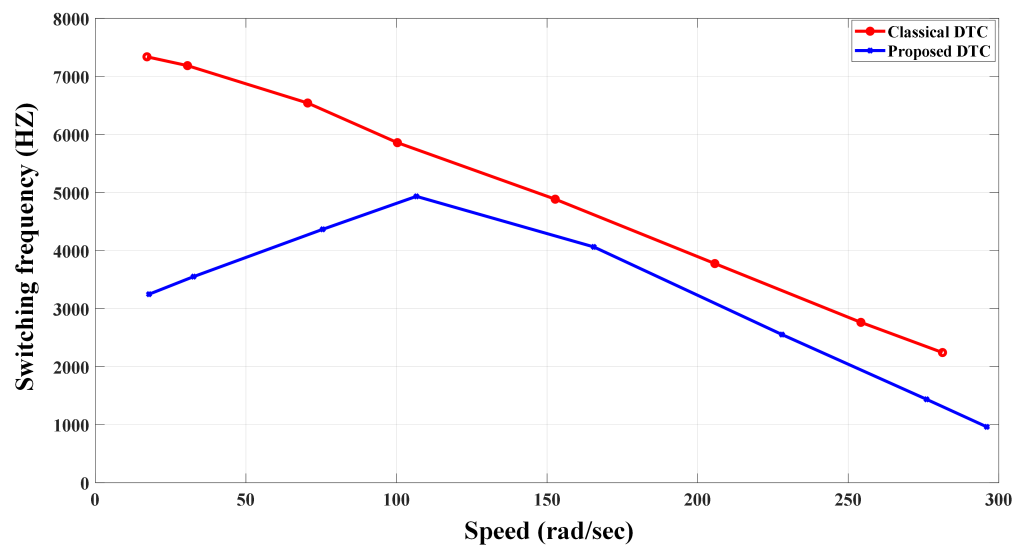
Figure 19. Switching frequency in both the classical and improved strategy.

5. Experimental Validation

Figure 20 shows the block diagram of the experimental platform used to test the proposed strategy in this research. The tested motor has the same parameters as those used in the simulation. Its nominal specifications with its parameters are fully explained in Appendix A. The dSPACE DS1103 digital processing card is used in order to perform all calculations and control requirements. The two current phases of the motor are measured using hall-effect sensors. The third phase current is calculated from the two measured currents. The dc link voltage of the power inverter is also measured. The measured values are entered into the Analog to Digital Converters (ADCs) units of the digital processing card. The stator current vector components are calculated using the Park matrix. In addition, the stator voltage vector components are calculated using the Equations (2) and (3). A control and monitoring interface was built within the dSPACE-supported ControlDesk software environment using the Host PC. This interface allows the application of the reference values of stator flux and torque. In addition, allowing monitoring of all state variables in real time. The interface and the dSPACE card are communicated using Real Time Interface units RTIs. However, the state variables such as currents and voltages can be monitored using oscilloscope after being processed through the digital to analog units DACs.
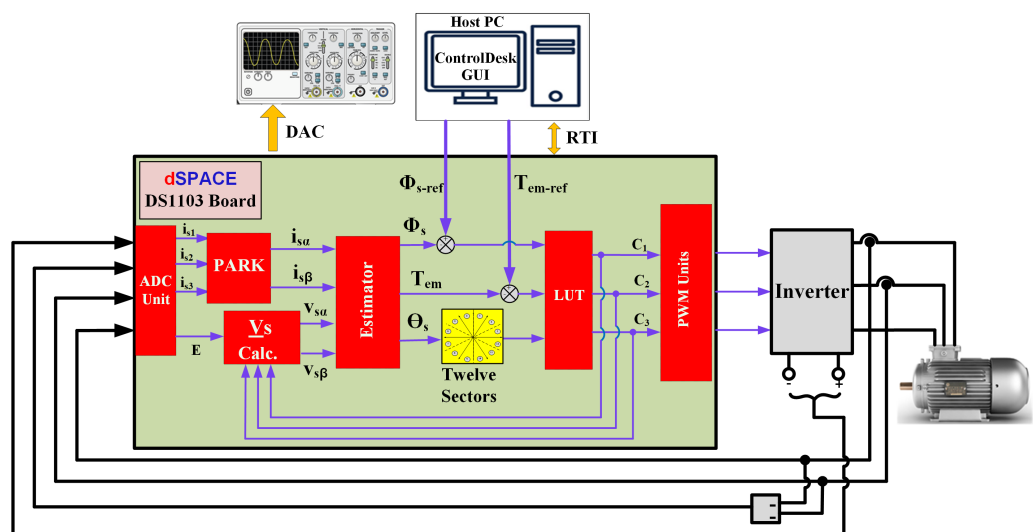

Figure 20. Practical block diagram of the experimental platform.

Figure 21 shows the results of the practical implementation of the six sectors of classical DTC for a sampling time of T_s = 50 microseconds. The electromagnetic torque was regulated around the nominal reference value of 1.76 N·m. In addition, the flux stator modulus was regulated around its nominal reference value of 1.14 Wb. It is observed that the currents suffer from large distortions and the torque suffers from a large value of the ripples equal to 1 N·m (56% of the nominal value). This excessive rise in torque ripples is explained by the use of the traditional integrator at the stage of the estimation block and the lack of online tracking of the stator resistance value. Figure 22 shows the results of the practical implementation of the improved twelve sectors strategy for a sampling time of T_s = 50 microseconds. A jump is made in the reference torque starting from half the nominal torque 0.88 N·m. At the moment 3.195 s, a reference value equal to the nominal torque 1.76 N·m is requested. It is noted that the regulation process is well around the reference values with high dynamics. In the same figure, the reference value of the nominal flux 1.14 Wb was requested, and the magnetic stator flux was well organized around the mentioned reference value with different jumps of the reference torque. The motor currents were sinusoidal with lower ripples compared to the classical strategy. However, they suffer from some distortions due to the presence of hysteresis regulators in the drive system. The twelve sectors of the stator flux path were plotted to ensure that the algorithm worked correctly over the entire operating range.
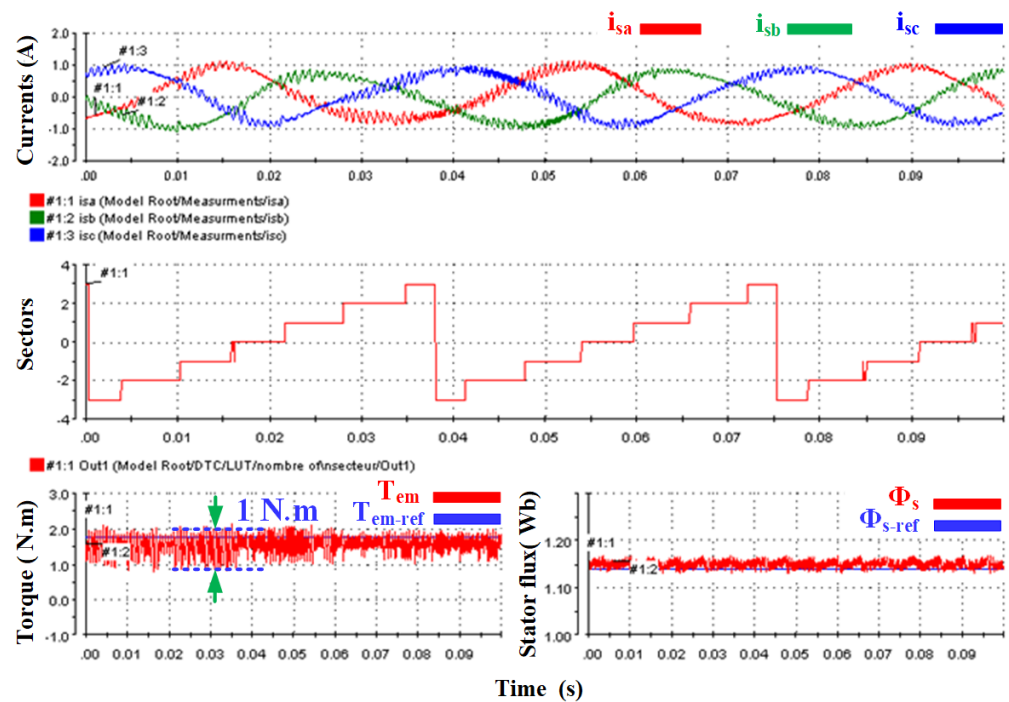

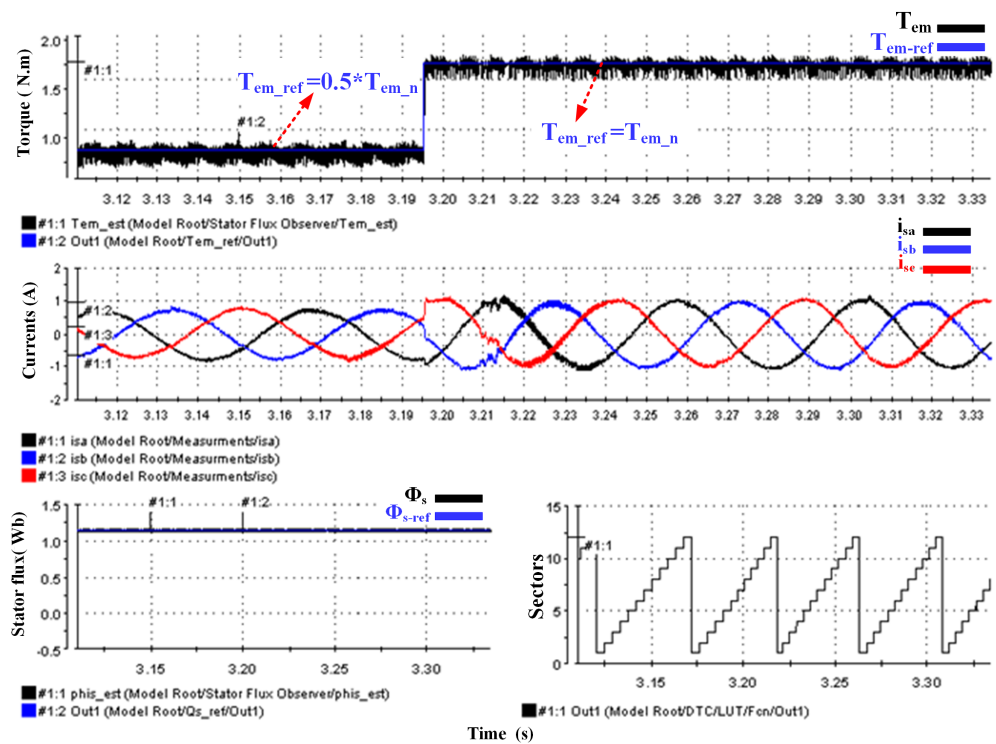**Figure 21.** Experimental results of the classical DTC algorithm.

Figure 22. Experimental results of the improved twelve sectors based DTC algorithm.

Figure 23 shows toque ripples and dynamics in the improved twelve sectors strategy at transient and steady state. It is illustrated that the value of the torque ripples is 0.2 N·m, which is significantly less than the torque ripples in the classical DTC strategy. In addition, the dynamics of the torque is obviously fast and equals 0.65 ms. These values confirm the clear improvement in the proposed strategy with the traditional strategy. Figure 24 shows the response of both the stator flux and the rotor flux. It is noted that the stator flux is well organized as we mentioned. However, the rotor flux is not regulated and fluctuates around the value 1.05 Wb.

Figure 25 shows the response of the components of the stator current vector, the stator flux vector, and the rotor flux vector, respectively in the stationary reference frame for the nominal values of torque and stator flux. It is noted that all these components are periodic sinusoidal with few distortions, and each real component is shifted from the imaginary component by 90 degrees [30].

Figure 26 shows the two components of the stator voltage vector in stationary reference frame. These components are periodic pulsating waveforms since they are calculated from the pulses of inverter in which the principle of direct drive is applied. These two components were calculated according to Equations (2) and (3).
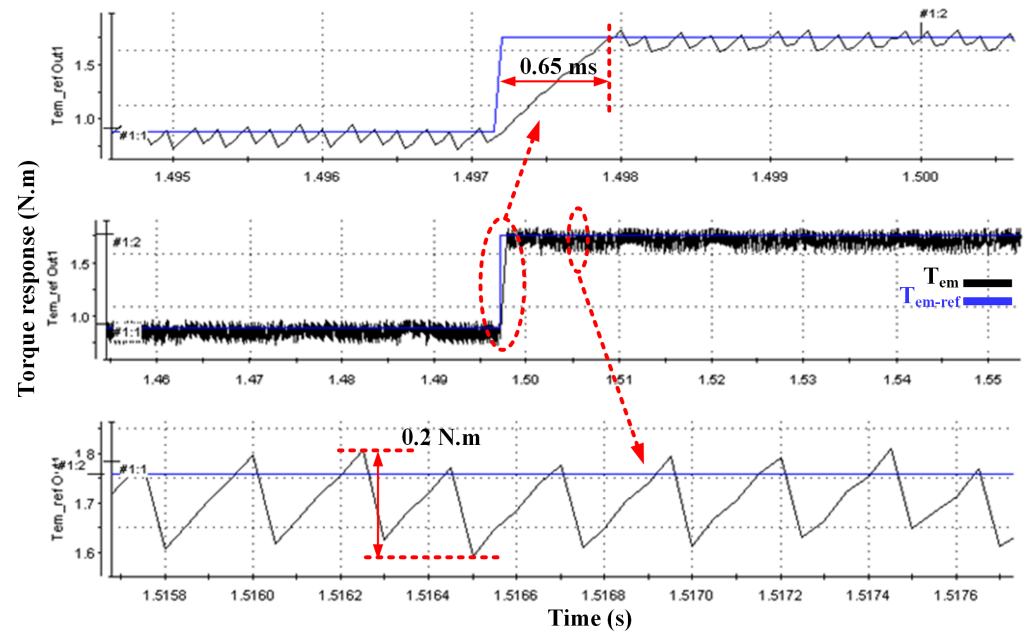
Figure 23. Experimental results of the torque ripples of the improved strategy.
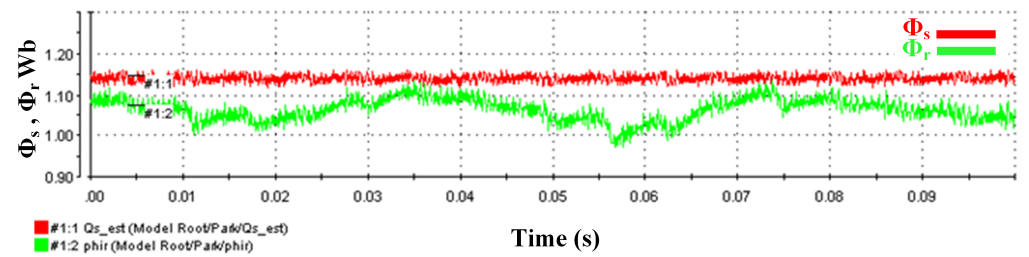

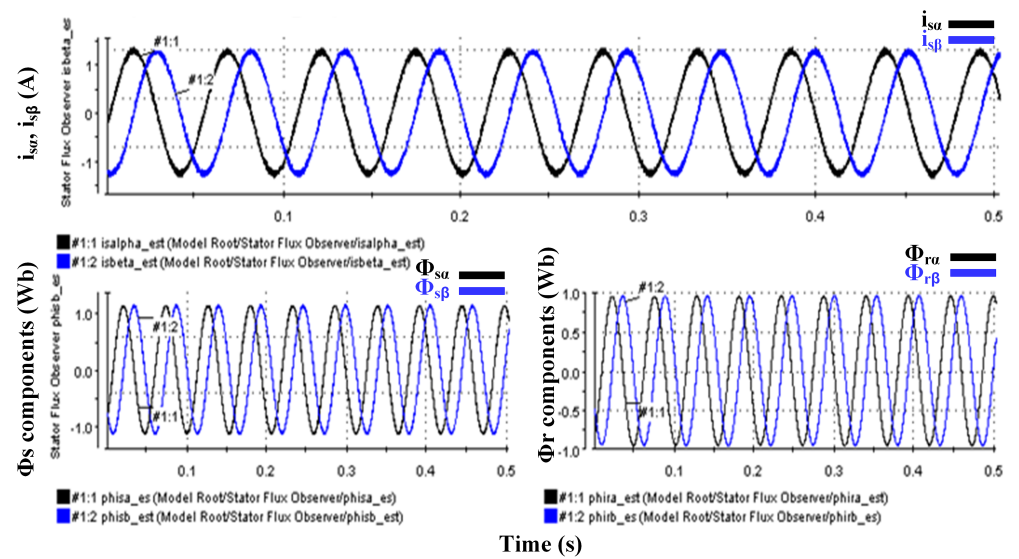**Figure 24.** Experimental results of the stator and rotor flux responses of the improved strategy.

Figure 25. Experimental results of the stator current, stator flux, and rotor flux components of the improved strategy.
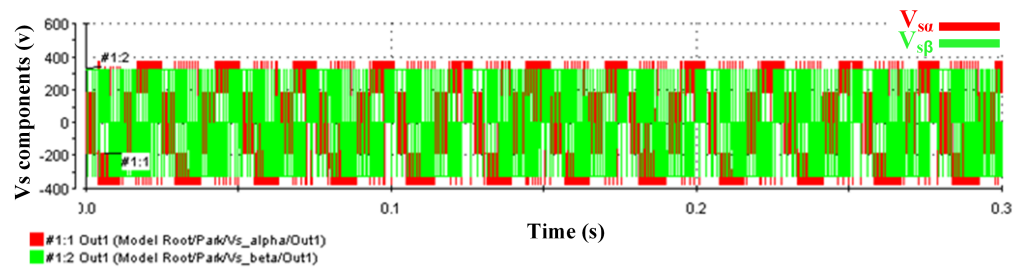
Figure 26. Experimental results of the stator voltage components of the improved strategy.

6. Comparison of the Proposed Strategy with the Classical DTC

In Table 3, the performance of the improved strategy is compared with the classical one. The comparison was performed for several parameters to confirm the superiority of the proposed strategy.

Table 3. Fair comparison between the improved and the classical strategy.

Operating Parameters Values	Classical DTC	Proposed Strategy
Torque ripples	0.6 N·m	0.15 N·m
Torque dynamic	0.5 ms	0.4 ms
Flux ripples	0.06 Wb	0.04 Wb
Torque dynamic	7 ms	4 ms
Switching frequency	7.25 to 2.1 kHz	3.1 to 1.2 kHz
Parameters variations	Weak	Strong
Lookup table construction	Designer's knowledge	Analytically
Computational time	17 μs	20 μs
Cost-effective	Low	Low

From Table 3, it can be noticed that the proposed strategy produces less torque ripples with higher dynamics. Similarly, the stator flux is produced with lower ripples and higher dynamics. The switching frequency in the proposed strategy is lower than in the conventional strategy over the entire speed range. With regard to the robustness towards the change of R_s, the proposed strategy is more robust, especially at low speeds. With regard to the switching table, its construction depends on the analytical investigation, while depends on the experience of the designer in the classical strategy which may not always be correct. The practical equipment for implementing the improved strategy did not differ from the classical one, which means that the computational time for the improved one did not increase much. Thus, its cost remains low.

7. Conclusions

In this research, an improved twelve based DTC strategy was presented by adopting an in-depth analytical study as a basis for the improvement process. The performance of the proposed strategy has been tested over the entire range of operation in order to ensure its effectiveness and robustness. The analytical investigation and simulation results were supported by the practical experiments on a dSPACE -based platform. The most important contributions achieved in this research can be summarized:

1. An in-depth analysis of the effects of voltage vectors on each of the flux and the torque was carried out for different loads and different values of stator resistance in order to obtain full comprehensive knowledge in choosing the switching table accurately.
2. The effect of zero voltage vector on both torque and flux is precisely determined over the entire speed range at no load and at full load.
3. A significant reduction in torque ripples has been achieved compared to the conventional strategy by more than 75%.
4. 20% faster dynamic torque response was achieved in the improved strategy compared to the classical strategy.

5. A significant reduction in magnetic flux ripples has been achieved by 33–50% depending on the value of the applied reference torque.
6. A faster dynamic was achieved in the flux response in the improved strategy compared to the traditional strategy by 40%.
7. A good reduction in stator current ripples has been achieved compared to the traditional strategy.
8. The robustness of the proposed strategy towards stator resistance variations has been proven, especially at low speeds that are very close to zero.
9. A clear reduction in the switching frequency of the inverter switches has been achieved over the entire speed range by 40–50% depending on the speed operation range.
10. The implementation of the improved strategy did not result in significant computational time compared to the classical strategy.
11. The improved strategy maintained simplicity and low cost due to no need for additional equipment.

Author Contributions: Conceptualization, M.M.A. and M.M.E.; methodology, M.M.A., I.M.A. and M.M.E.; software, M.M.A.; validation, M.M.A., I.M.A. and M.M.E.; formal analysis, M.M.A. and M.M.E.; investigation, M.M.A., I.M.A. and M.M.E.; resources, M.M.A. and M.M.E.; data curation, M.M.A.; writing—original draft preparation, M.M.A. and M.M.E.; writing—review and editing, M.M.A., I.M.A. and M.M.E.; visualization, M.M.A., I.M.A. and M.M.E.; supervision, M.M.A., I.M.A. and M.M.E.; project administration, M.M.A., I.M.A. and M.M.E.; funding acquisition, M.M.A., I.M.A. and M.M.E. All authors have read and agreed to the published version of the manuscript.

Appendix A

Table A1. The IM nameplate data and parameters.

Variable	Unit value
Nominal voltage	230/400 V
Phase resestance stator	$R_s = 45.83\ \Omega$
Phase resestance rotor	$R_r = 31\ \Omega$
Phase inductance stator	$L_s = 1.24$ H
Phase inductance rotor	$L_r = 1.11$ H
Mutual inductance	$L_m = 1.05$ H
Inertia	$J = 0.006\ \text{kg} \cdot \text{m}^2$
Friction factor	$F = 0.001\ \text{N} \cdot \text{m} \cdot \text{s/rad}$
Number of poles pairs	$P = 2$
Nominal stator flux	$\Phi_s = 1.14$ Wb
Nominal rotor flux	$\Phi_r = 0.945$ Wb
Nominal power	$P_n = 0.25$ kW
Nominal frequency	$F = 50$ Hz
Nominal speed	$\omega_n = 282$ rad/s
Nominal torque	$T_{em} = 1.76\ \text{N} \cdot \text{m}$

References

1. Takahashi M.; Noguchi T. A New Quick-Response and High- Effecincy Control Strategy of an Induction Motor. *IEEE Trans. Ind. Appl.* **1986**, *IA-22*, 820–827. [CrossRef]
2. Depenbrock, M. Direct Self-Control (DSC) of inverter-fed induction machine. In Proceedings of the IEEE Power Electronics Specialists Conference, Blacksburg, VA, USA, 21–26 June 1987. [CrossRef]

3. Bojoi, R.; Farina, F.; Griva, G.; Profumo, F.; Tenconi, A. Direct torque control for dual three-phase induction motor drives. *IEEE Trans. Ind. Appl.* **2005**, *41*, 1627–1636. [CrossRef]

4. Martins, C.A.; Roboam, X.; Meynard, T.A.; Carvalho, A.S. Switching frequency imposition and ripple reduction in DTC drives by using a multilevel converter. *IEEE Trans. Power Electron.* **2002**, *17*, 286–297. [CrossRef]

5. Shaobang, X.; Yinsheng, L. PMSM twelve sectors DTC system with minimum iron loss. In Proceedings of the 2011 International Conference on Electric Information and Control Engineering, Wuhan, China, 15–17 April 2011; pp. 1542–1545. [CrossRef]

6. Yan, H.; Yang, J.; Zeng, F. Three-Phase Current Reconstruction for PMSM Drive With Modified Twelve Sector Space Vector Pulse Width Modulation. *IEEE Trans. Power Electron.* **2022**, *37*, 15209–15220. [CrossRef]

7. Haissouf, M.E.; Haroussi, M.E.; Ba-Razzouk, A. DSP In the Loop implementation of an enhanced Direct Torque Control for Induction Motor drive. In Proceedings of the 2nd International Conference on Innovative Research in Applied Science, Engineering and Technology (IRASET), Meknes, Morocco, 3–4 March 2022. [CrossRef]

8. Manuprasad, P.; Mohanty, K.B. Implementation of 12 Sector Fuzzy Controller for Direct Torque Control of Induction Motor. In Proceedings of the 2019 Innovations in Power and Advanced Computing Technologies (i-PACT), Vellore, India, 22–23 March 2019; pp. 1–6. [CrossRef]

9. Meesala, R.E.K.; Thippiripati, V.K. An Improved Direct Torque Control of Three-Level Dual Inverter Fed Open-Ended Winding Induction Motor Drive Based on Modified Look-Up Table. *IEEE Trans. Power Electron.* **2020**, *35*, 3906–3917. [CrossRef]

10. Hakami, S.S.; Lee, K.B. Four-level hysteresis-based DTC for torque capability improvement of IPMSM fed by three-level NPC inverter. *Electronics* **2020**, *9*, 1558. [CrossRef]

11. Mahmud, M.H.; Wu, Y.; Alhosaini, W.; Diao, F.; Zhao, Y. Enhanced Direct Torque Control for a Three-Level T-Type Inverter. *IEEE Trans. Transp. Electrif.* **2021**, *7*, 1638–1651. [CrossRef]

12. Bhangale, S.V.; Kumar, R.; Bhangale, K. 18-Sector Direct Torque Controlled Strategy with Improved Stator Flux Estimator for Induction Motor Drive. In Proceedings of the 2018 8th IEEE India International Conference on Power Electronics (IICPE), Jaipur, India, 13–15 December 2018; pp. 1–6. [CrossRef]

13. Suresh, S.; Rajeevan, P.P. Virtual Space Vector-Based Direct Torque Control Schemes for Induction Motor Drives. *IEEE Trans. Ind. Appl.* **2020**, *56*, 2719–2728. [CrossRef]

14. Alsofyani, I.M.; Bak, Y.; Lee, K.-B. Fast Torque Control and Minimized Sector-Flux Droop for Constant Frequency Torque Controller Based DTC of Induction Machines. *IEEE Trans. Power Electron.* **2019**, *34*, 12141–12153. [CrossRef]

15. Jidin, A.; Idris, N.R.N.; Yatim, A.H.M.; Sutikno, T.; Elbuluk, M.E. An Optimized Switching Strategy for Quick Dynamic Torque Control in DTC-Hysteresis-Based Induction Machines. *IEEE Trans. Ind. Electron.* **2011**, *58*, 3391–3400. [CrossRef]

16. Alsofyani, I.M.; Idris, N.R.N.; Lee, K.-B. Dynamic Hysteresis Torque Band for Improving the Performance of Lookup-Table-Based DTC of Induction Machines. *IEEE Trans. Power Electron.* **2018**, *33*, 7959–7970. [CrossRef]

17. Alsofyani, I.M.; Lee, K.-B. Enhanced Performance of Constant Frequency Torque Controller–Based Direct Torque Control of Induction Machines with Increased Torque-Loop Bandwidth. *IEEE Trans. Ind. Electron.* **2020**, *67*, 10168–10179. [CrossRef]

18. Bouhoune, K.; Yazid, K.; Boucherit, M.S.; Menaa, M. Fuzzy logic-based direct torque control for induction machine drive. In Proceedings of the 2017 25th Mediterranean Conference on Control and Automation (MED), Valletta, Malta, 3–6 July 2017; pp. 577–582. [CrossRef]

19. Chaikhy, H.; Khafallah, M.; Saad, A.; Chikh, K.; Es-Saadi, M. Comparison between classical and intelligent DTC strategies for induction machine. In Proceedings of the 2012 International Conference on Multimedia Computing and Systems, Tangiers, Morocco, 10–12 May 2012; pp. 1163–1167. [CrossRef]

20. Elgbaily, M.; Anayi, F.; Packianather, M. Performance Improvement Based Torque Ripple Minimization for Direct Torque Control Drive Fed Induction Motor Using Fuzzy Logic Control. In *Control, Instrumentation and Mechatronics: Theory and Practice*; Springer Nature: Singapore, 2022; pp. 416–428. [CrossRef]

21. Elgbaily, M.; Anayi, F.; Packianather, M. Genetic and particle swarm optimization algorithms based direct torque control for torque ripple attenuation of induction motor. *Mater. Today Proc.* **2022**, *67*, 577–590. [CrossRef]

22. Eial, Awwad, A. Dynamic Performance Enhancement of a Direct-Driven PMSG-Based Wind Turbine Using a 12-Sectors DTC. *World Electr. Veh. J.* **2022**, *13*, 123. [CrossRef]

23. Idris, N.R.N.; Yatim, A.H.M. Direct torque control of induction machines with constant switching frequency and reduced torque ripple. *IEEE Trans. Ind. Electron.* **2004**, *51*, 758–767. [CrossRef]

24. Bertoluzzo, M.; Buja, G.; Menis, R. Direct torque control of an induction motor using a single current sensor. *IEEE Trans. Ind. Electron.* **2006**, *53*, 778–784. [CrossRef]

25. Buja, G.; Menis, R. Steady-State Performance Degradation of a DTC IM Drive Under Parameter and Transduction Errors. *IEEE Trans. Ind. Electron.* **2008**, *55*, 1749–1760. [CrossRef]

26. Naassani, A.A.; Monmasson, E.; Louis, J.-P. Synthesis of direct torque and rotor flux control algorithms by means of sliding-mode theory. *IEEE Trans. Ind. Electron.* **2005**, *52*, 785–799. [CrossRef]

27. Naassani, A.A.; Monmasson, E.; Louis, J.-P. Dynamic reconfiguration of direct torque and stator flux control by means of sliding mode theory. In Proceedings of the European Conference on Power Electronics and Applications, Dresden, Germany, 11–14 September 2005. [CrossRef]

28. Alshbib, M.M.; Elgbaily, M.; Anayi, F. An In-Depth Analytical Study of Switching States of Direct Torque Control Algorithm for Induction Motor over the Entire Speed Range. In Proceedings of the 1st International Electronic Conference on Machines and Applications (IECMA), Electronic Conferences, 15–30 September 2022. [CrossRef]
29. Alshbib, M.M.; Elgbaily, M.M.; Alsofyani, I.M.; Anayi, F. Performance Enhancement of Direct Torque and Rotor Flux Control (DTRFC) of a Three-Phase Induction Motor Over the Entire Speed Range: Experimental Validation. *Machines* **2023**, *11*, 22. [CrossRef]
30. Elgbaily, M.; Anayi, F.; Alshbib, M.M. A combined control scheme of direct torque control and field-oriented control algorithms for three-phase induction motor: Experimental validation. *Mathematics* **2022**, *10*, 3842. [CrossRef]